The Tropical Rainfall Measuring Mission (TRMM) Sensor Package

CHRISTIAN KUMMEROW AND WILLIAM BARNES

NASA/Goddard Space Flight Center, Greenbelt, Maryland

TOSHIAKI KOZU

Communications Research Laboratory, Tokyo, Japan

JAMES SHIUE AND JOANNE SIMPSON

NASA/Goddard Space Flight Center, Greenbelt, Maryland

3 July 1997 and 1 August 1997

ABSTRACT

This note is intended to serve primarily as a reference guide to users wishing to make use of the Tropical Rainfall Measuring Mission data. It covers each of the three primary rainfall instruments: the passive microwave radiometer, the precipitation radar, and the Visible and Infrared Radiometer System on board the spacecraft. Radiometric characteristics, scanning geometry, calibration procedures, and data products are described for each of these three sensors.

1. TRMM overview

The atmosphere gets three-fourths of its heat energy from the release of latent heat by precipitation, and an estimated two-thirds of this precipitation falls in the Tropics. Differences in large-scale rainfall patterns and their associated energy release in the Tropics, in turn, affect the entire global circulation, as manifested in El Niño events, to name just one example. The most important impact of rain and its variability is on the biosphere, including humans. The ''average'' rainfall is rarely observed. Instead, several seasons of drought and starvation are often followed by a year or two of torrential downpours and disastrous floods. Quantitative estimates of tropical precipitation, unfortunately, still vary by as much as 100%, depending upon the estimates. These differences are due to both the lack of good direct measurements of rainfall, as well as the highly variable nature of the parameters both spatially and temporally.

Cloud and rain processes are now simulated fairly well on the scale of cloud ensembles (50–100 km). However, global models for prediction of weather and climate have much coarser resolution, therefore they must ''parameterize'' cloud processes. Most of these parameterizations are extremely crude. In the Tropics particularly, it is vitally important to have rain and its latent heating in the initialization of global weather and climate models, as well as in their prediction stage. Presently, there are large discrepancies among the results of the different models. All of these models inadequately predict precipitation and soil moisture. The poor simulation of cloud properties is one of the factors causing the models to differ so widely regarding the amount of global warming with doubled carbon dioxide. Scarcity of quantitative precipitation information has been a frustrating long-time bottleneck for atmospheric science. This gap in the center of the hydrologic cycle has had negative impacts on nearly all earth sciences and their applications. Since the Tropics are 75% covered with ocean, precipitation over the global Tropics can be measured satisfactorily only from space.

The Tropical Rainfall Measuring Mission (TRMM) is a joint mission between the National Aeronautics and Space Administration (NASA) of the United States and the National Space Development Agency (NASDA) of Japan. The objectives of TRMM are to measure rainfall and energy (i.e., latent heat of condensation) exchange of tropical and subtropical regions of the world. The primary rainfall instruments on TRMM are the TRMM Microwave Imager (TMI), the precipitation radar (PR), and the Visible and Infrared Radiometer System (VIRS). Additionally, the TRMM satellite will carry two related Earth Observing System (EOS) instruments in the Clouds and Earth's Radiant Energy System (CERES)

Corresponding author address: Dr. Christian D. Kummerow, Code 912, Laboratory for Atmospheres, NASA Goddard Space Flight Center, Greenbelt, MD 20771.
E-mail: Kummerow@audry.gsfc.nasa.gov

and the Lightning Imaging System (LIS). The space segment of TRMM is a satellite in a 350-km circular orbit with a 35° inclination angle. It was scheduled to be launched in the summer of 1997 with a mission life of at least 3 years.

The combination of satellite-borne passive and active sensors to be deployed in the upcoming TRMM promises to provide critical information regarding the three-dimensional distributions of precipitation and heating in the Tropics (Simpson et al. 1996). Coincident measurements from TMI and PR are complementary: passive microwave radiometers measure radiances that are the end product of the integrated effects of electromagnetic absorption–emission and scattering through the precipitating cloud along the sensor viewpath. The frequency dependence of electromagnetic properties of cloud and precipitation particles allows for the design of multichannel passive microwave radiometers that can ''sound'' to different depths in a precipitating cloud, but the height assignment of cloud properties is not very specific. On the other hand, active microwave sensors (radars) provide specific height information based upon the time delay of the precipitation-backscattered return power. However, simple one-parameter radars (such as the TRMM PR) only operate at one transmitting/receiving frequency and polarization. To obtain unambiguous precipitation water content profiles from these radars, secondary signal effects such as path attenuation must be determined independently.

The VIRS on TRMM adds cloud-top temperatures and structures to complement the description of the two microwave sensors. While direct precipitation information from VIRS is less reliable than that obtained by the microwave sensors, VIRS serves an important role as a bridge between the high quality but infrequent observations from TMI and PR with the more available data and longer time series data available from the geostationary VIS/IR satellite platforms.

The CERES and the LIS, while designated as EOS instruments, still play an important role in the TRMM mission to round out the scientific objectives. The lightning sensor (Goodman et al. 1996), aside from mapping the global frequency of lightning events, will play an important role in coupling the occurrence of lightning to the precipitation—thus enhancing our overall understanding of both lightning as well as precipitation processes. The CERES instrument (Wielicki et al. 1996) allows for determination of the total radiant energy balance. Together with the latent heating derived from the precipitation, a significantly improved picture of the atmospheric energy system can emerge.

A substantial number of recent scientific publications have dwelled upon the importance of TRMM, the development of rainfall algorithms, and the applications of TRMM data. The focus of this paper is on the measurements that will be made by the TRMM rainfall sensors. The subsequent sections describe each of the three primary rainfall instruments, their measurement characteristics, their scanning geometry, and their expected data products. Figure 1 presents an overview of the spacecraft scanning geometry showing the relative footprint locations of PR, VIRS, and TMI.

2. TRMM Microwave Imager (TMI)

The TMI is a nine-channel passive microwave radiometer based upon the Special Sensor Microwave/Imager (SSM/I), which has been flying aboard the U.S. Defense Meteorological Satellite Program (DMSP) satellites since 1987. The key differences are the addition of a pair of 10.7-GHz channels with horizontal and vertical polarizations and a frequency change of the water vapor channel from 22.235 to 21.3 GHz. This change off the center of the water vapor line was made in order to avoid saturation in the tropical orbit of TRMM. Table 1 presents the performance characteristics of the nine TMI channels. The increased spatial resolution evident in Table 1 is due to the lower orbit of the TRMM satellite with respect to the DMSP rather than sensor differences.

a. The antenna and conical scan

The TMI antenna is an offset parabola, with an aperture size of 61 cm (projected along the propagation direction) and a focal length of 50.8 cm. The antenna beam views the earth surface with a ''nadir'' angle of 49°, which results in an incident angle of 52.8° at the earth's surface. The TMI antenna rotates about a nadir axis at a constant speed of 31.6 rpm. The rotation draws a ''circle'' on the earth's surface. Only 130° of the forward sector of the complete circle is used for taking data. The rest is used for calibrations and other instrument housekeeping purposes. From the TRMM orbit, the 130° scanned sector yields a swath width of 758.5 km shown in Fig. 1. During each complete revolution (i.e., a scan period of about 1.9 s), the subsatellite point advances a distance d of 13.9 km. Since the smallest footprint (85.5-GHz channels) size is only 6.9 km (down-track direction) by 4.6 km (cross-track direction), there is a ''gap'' of 7.0 km between successive scans. However, this is the only frequency where there is a small gap. For all higher-frequency channels, footprints from successive scans overlap the previous scans. The ''footprint'' size here is the effective field of view (EFOV); its definition is explained in section 2b.

b. The effective field of view (EFOV)

The instantaneous field of view (IFOV) is the footprint resulting from the intersection of antenna beamwidth (taken to be between the 3 dB, or half power points) and the earth's surface. Due to the shape of the antenna itself, and the off-nadir incidence angle at the surface, the resulting pattern at the earth's surface can be described by an ellipse. The ellipse's minor diameter is in the scanning or cross-track direction, called the

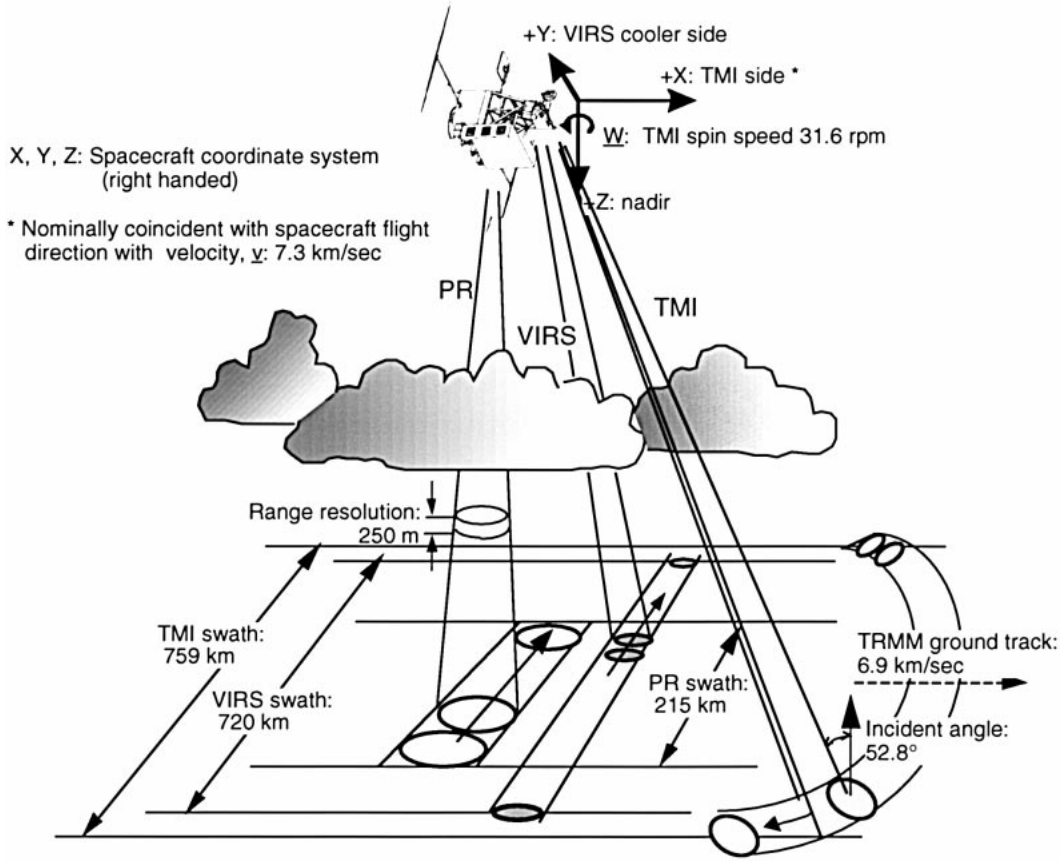

FIG. 1. Schematic view of the scan geometries of the three TRMM primary rainfall sensors: TMI, PR, and VIRS.

IFOV-CT, while the major diameter is in the down-track direction called IFOV-DT.

Because the TMI is rotating while its receiver is integrating, the concept of effective field of view (EFOV) must be introduced. It is the effective area swept by the antenna beam during the integration time, as shown in Fig. 2. For the 85.5-GHz channels, its beam moves from its starting position along the scan direction one IFOV-CT in distance. The EFOV is taken to be the heavy ellipse centered between the two IFOVs. The center of

TABLE 1. TMI characteristics. Beam efficiency is the percentage of power enclosed within 2.5 times the beamwidth. Cross polarization is the percentage power contributed by the cross-polarized component to the main beam. (Mass: 65 kg, power: 50 W, and data rate: 8.5 kbps)

Channel number	1	2	3	4	5	6	7	8	9
Center freq (GHz)	10.65	10.65	19.35	19.35	21.3	37.0	37.0	85.5	85.5
Polarization	V	H	V	H	V	V	H	V	H
Bandwidth (MHz)	100	100	500	500	200	2000	2000	3000	3000
Stability (MHz)	10	10	20	20	20	50	50	100	100
Beamwidth (deg)	3.68	3.75	1.90	1.88	1.70	1.00	1.00	0.42	0.43
IFOV-DT (km)	59.0	60.1	30.5	30.1	27.2	16.0	16.0	6.7	6.9
IFOV-CT (km)	35.7	36.4	18.4	18.2	16.5	9.7	9.7	4.1	4.2
Integration time per sample (ms)	6.60	6.60	6.60	6.60	6.60	6.60	6.60	3.30	3.30
EFOV-CT (km)	9.1	9.1	9.1	9.1	9.1	9.1	9.1	4.6	4.6
EFOV-DT (km)	63.2	63.2	30.4	30.4	22.6	16.0	16.0	7.2	7.2
EFOVs per scan	104	104	104	104	104	104	104	208	208
Samples (N) per beamwidth	4	4	2	2	2	1	1	1	1
Beam EFOV (km × km)	63 × 37	63 × 37	30 × 18	30 × 18	23 × 18	16 × 9	16 × 9	7 × 5	7 × 5
Beam EFOVs per scan	26	26	52	52	52	104	104	208	208
Temperature sensitivity, NEΔT (K)	0.63	0.54	0.50	0.47	0.71	0.36	0.31	0.52	0.93
Beam temperature sensitivity NEΔT (K)	0.32	0.27	0.35	0.33	0.50	0.36	0.31	0.52	0.93
Beam efficiency/Xpol(%)	93/0.4	93/0.5	96/0.4	96/0.5	98/0.6	91/2.2	92/2.1	82/2.0	85/3.0

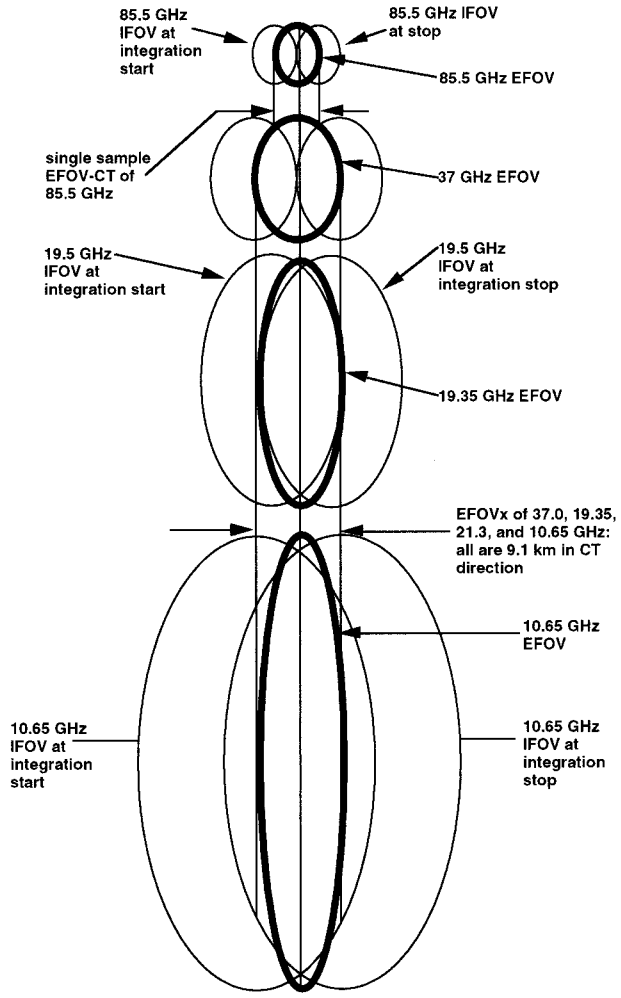

FIG. 2. TRMM Microwave Imager footprint characteristics.

the EFOV is the position of the antenna beam at the midpoint of the integration period. The EFOVs of other frequencies are defined similarly. Notice, however, that for the 85.5- and 37.0-GHz channels, the EFOV is almost the same size as the IFOV. This is because the lengths of (nominal) integration time (a.k.a., ''single sample integration time'') are chosen to be 3.3 and 6.6 ms, respectively, which are the times needed for their respective beams to move one IFOV distance. However, the same 6.6-ms nominal integration time length is used for all the rest of the lower frequencies. Their EFOV-CTs are thus 9.1 km, regardless of their actual beamwidths. The EFOVs shown in Fig. 2 are called single-sample EFOVs because they are the results of only one integration time period or ''one sample.''

Satellite movement in the down-track direction is very small during the millisecond integration time. In the down-track direction, the EFOV-DTs are therefore taken to be the same as the IFOV-DT. With these definitions, the size of the EFOV-CTs for lower frequencies appears to be ''artificially too narrow'' as compared to their respective IFOVs. It is important to note that it is this artificially narrow EFOV-CT that will be provided as the standard TMI brightness temperature data. One can also define a ''beam'' EFOV-CT by joining a number (N) of neighboring single-sample EFOVs (in the CT direction) together to form an equivalent beam EFOV or BEFOV. Using the values of N listed in Table 1 will result in BEFOV CTs, which are comparable in size to the IFOV CTs. The values of N range from 2–4.

In summary, the TMI data will be provided at the single-sample EFOV level, but for those frequencies (10.7, 19.4, and 21.3 GHz) that contain more than one sample per beam width, the user can reprocess the data into equivalent BEFOVs, which are then the same size as the IFOVs given by the antenna beamwidths. The BEFOVs represent the true resolution (or footprints) of the TMI.

c. Onboard calibration

At the end of the 130° active earth-viewing part of the scan, the TMI goes through a two-point calibration process, which consists of one look each at a ''hot'' and a ''cold'' reference temperature. During the hot calibration, the feed horns are moved to a position viewing a ''hot load'' whose brightness temperature is known accurately. Next, the feed horns are moved to a second position where their beams are reflected by a ''cold space subreflector'' to view the cosmic background radiation. The two-point calibration is repeated every scan period to establish the instantaneous calibration of the TMI and remove any gain fluctuation effects. The frequent onboard calibration is a key to preserving the stability of the TMI, which is a total power-type microwave radiometer.

d. TMI standard data products

The standard level 1B TMI data will be given as single-sample EFOVs. They will be the ''calibrated'' microwave brightness temperatures (using the appropriate onboard calibration data) for that EFOV and corrected for the cross-polarization effect. Each scan line will contain the time of the scan line, along with data quality indicators and a TRMM direction indicator. Unlike the SSM/I satellites, it will be necessary to occasionally rotate the TRMM spacecraft by 180° to maintain thermal balance. The TMI beam may therefore either precede or follow the TRMM subsatellite point. The earth science data in each scan line will consist of latitude and longitude values along with brightness temperatures for the 208 EFOVs at 85 GHz and 104 EFOVs at all the remaining lower-frequency channels. Along the scan direction, EFOVs of all frequencies are coaxial and the EFOV-CTs are of the same size (i.e., 9.1 km, except for the 85-GHz channels that are spaced 4.6 km apart). All scan lines are identical. TMI does not differentiate into ''A'' and ''B'' scans as do the SSM/I.

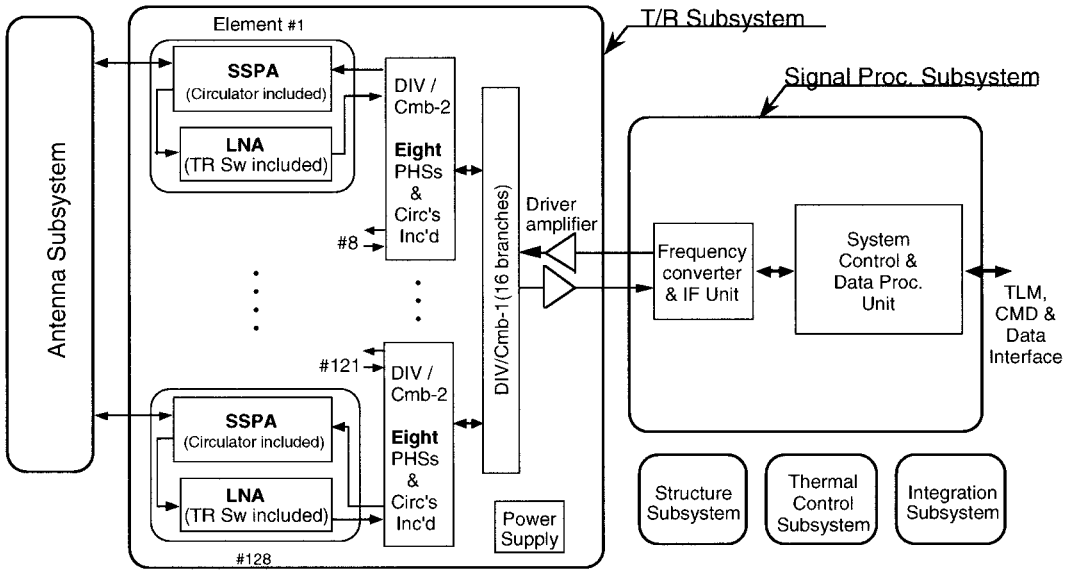

FIG. 3. Precipitation radar block diagram.

Data will be granularized into one-orbit elements with orbits beginning at the southernmost satellite subtrack. Each granule of TMI data will be padded with 50 scan lines before and after the actual orbit. This was done to facilitate the merging of TMI data with the PR and VIRS instrument data described in section 3.

3. Precipitation radar (PR)

The PR will be the first rain radar in space. Its key goals can be summarized as 1) providing three-dimensional structure of rainfall, particularly of the vertical distribution; 2) obtaining quantitative rainfall measurements over land as well as over ocean; and 3) improving the overall TRMM precipitation retrieval accuracy by combined use of active (PR) and passive (TMI and VIRS) sensor data. The PR has been developed by NASDA in cooperation with Communications Research Laboratory, Ministry of Posts and Telecommunications.

TABLE 2. Major parameters of TRMM PR.

Item	Specification
Frequency	13.796, 13.802 GHz
Sensitivity	$\leq\sim$0.7 mm h^{-1} (S/N/pulse $\approx$ 0 dB)
Swath width	215 km
Observable range	Surface to 15-km altitude
Horizontal resolution	4.3 km (nadir)
Vertical resolution	0.25 km (nadir)
Antenna	
Type	128-element WG planar array
Beamwidth	0.71° × 0.71°
Aperture	2.0 m × 2.0 m
Scan angle	±17° (Cross-track scan)
Transmitter/receiver	
Type	SSPA and LNA (128 channels)
Peak power	≥500 W (at antenna input)
Pulse width	1.6 μs × 2 ch. (transmitted pulse)
PRF	2776 Hz
Dynamic range	≥70 dB
Number of independent samples	64
Data rate	93.2 kbps

a. System description

The PR is a 128-element active phased array system operating at 13.8 GHz. A functional block diagram is shown in Fig. 3. The transmitter/receiver (T/R) consists of 128 solid-state power amplifiers (SSPAs), LNAs, and PIN-diode phase shifters (PHSs). Actually, the PHS is included in the divider/combiner-2 (DIV/CMB-2). Each T/R element is connected to a 2-m slotted waveguide antenna, by which a 2 m × 2 m planar array is constructed. To achieve low antenna sidelobe levels (i.e., to suppress sidelobe-coupled surface clutter), SSPA output powers and LNA gains are weighted to achieve the Taylor distribution (SL = −35 dB, $\bar{n}$ = 6) with a 1-dB quantization. Parameters of the PR are listed in Table 2. The mechanical structure of the PR is about 2.3 m × 2.3 m × 0.7 m in size and consists of the platform and the antenna. The antenna substrate is attached to the platform by a kinematic mounting technique to prevent an antenna pattern degradation caused by mechanical and thermal distortion of the antenna.

The PR uses a frequency agility technique to obtain 64 (N_s = 64) independent samples with a fixed pulse repetition frequency of 2776 Hz, in which a pair of 1.6-μs pulses differing in frequency by 6 MHz are transmitted. Thirty-two pairs of pulses are transmitted for each of 49 angle bins with the angle-bin interval of 0.71°

TABLE 3. Summary of PR operation modes.

PR mode	Description
Observation	Nominal science observation, ±17° cross-track scan
External calibration	Special oversample scan (center scan angle ±1.1°) or fixed beam position
Internal calibration	Internal-loop calibration for receiver I-O transfer function measurement
Standby	Temporal RF radiation stop, phase-shifter data load and dump
Analysis	LNA functional check using surface return
Health check	Onboard computer ROM/RAM function check
Safety	PR power off

TABLE 4. Outline of radar echo collection parameters.

Type of radar echo	Description
Nominal rain and surface echoes	Surface to 15-km altitude, 250-m interval, all scan angles
Mirror image	0–5-km altitude, 250-m interval, at nadir only
Oversampled surface echo	Surface echo peak ±0.5 km, 125-m interval, scan angles within ±10°
Oversampled rain echo	Surface echo peak to 7.5-km altitude, 125-m interval, scan angles within ±3.5°

over the 215-km swath. The observation concept of the PR is illustrated in Fig. 1.

b. Operation mode

Table 3 summarizes the operation modes of the PR. Nominally, the PR is operated in the observation mode where the PR antenna scans in the cross-track direction over ±17° (215-km swath). Periodically, the PR performs an external calibration with an Active Radar Calibrator (ARC) and an internal loop calibration to measure the transfer function of the PR receiver. Other modes include the standby mode (to stop the RF radiation temporarily and upload the phase-shifter data to PR), the analysis mode (to monitor the function of 128 LNAs), and the health check mode (to check the function of onboard CPU memories). The precipitation radar along-track antenna pattern can be measured in the ARC calibration. The cross-track pattern can also be measured with the ARC by employing a special spacecraft attitude (90° yaw maneuver). This will be performed during the initial TRMM check-out phase.

Antenna array weights will be monitored using the SSPA power monitor telemetries and the data obtained from the PR analysis mode. In the analysis mode, each of the 128 LNAs will be activated for a 0.6-s period, and the surface echo level will be measured using the LNA. This is repeated 128 times to verify that each LNA is operating normally and to obtain an estimate of receive antenna amplitude weighting.

c. Radar echo collection scheme

The radar echo of PR consists of the following three components: rain echo, surface echo, and mirror image echo. The surface echo is measured because of the importance of the surface echo for estimating the total path attenuation (Meneghini and Kozu 1990) and to provide the range of the surface along the radar beam. The mirror image, which is the rain echo received through the double reflection at the surface, may prove useful for certain rainfall rate retrieval schemes. It is measured at nadir incidence. Near nadir, the data are further oversampled (125-m intervals) in order to improve the retrieval of echo profiles that have high spatial frequency (surface return and bright band). Major parameters of radar data collection are summarized in Table 4.

Independent measurement of system noise level is performed for each angle bin in order to estimate radar echo power from the total (echo plus noise) received power. For this measurement, a total of four range bins are allocated, where sidelobe-coupled surface clutter and rain echo should be negligible. This results in 256 independent samples for system noise. Using this system noise measurement, effective signal-to-noise ratio (Meneghini and Kozu 1990) of about 4 dB is obtained at the rain rate of 0.7 mm h^{-1}.

d. Data processing

Precipitation radar data are archived as level 1B and level 1C. The level 1B data follow the standard definition of the instrument data with appended geolocation information. In the case of the PR, the level 1B data contain returned power and noise levels. Level 1C was developed primarily to reduce the volumes of radar data for precipitation applications. To that end, the power and noise values are converted to an apparent reflectivity (i.e., no attenuation correction is applied). Furthermore, all pixels that do not exceed the rainfall threshold of 15 dBZ (well below the sensitivity of the PR) are omitted. In this manner, the approximately 2.2 Gbyte day^{-1} of PR level 1B data will be reduced to approximately 450 Mbyte day^{-1}. All geophysical products, including 3D rain-rate maps, qualitative rain characteristics (rain type, storm top, and brightband heights), and statistics of surface scattering cross sections from nadir to 17° incidence angles (Okamoto and Kozu 1993) are computed from the level 1 data products.

e. Calibration strategy

Accurate calibration of the PR is important to establish the clear interface condition between level 1 and higher-level algorithms, thereby ensuring accurate and stable rain products. To develop the PR calibration algorithm, variation and drift of PR system parameters are modeled to have ''intermediate-term'' and ''long-

TABLE 5. VIRS performance parameters.

Channel	λ (μm)	$\Delta\lambda$ (μm)	Nominal radiance [mW (cm^2 sr μm)$^{-1}$]	Maximum radiance [mW (cm^2 sr μm)$^{-1}$]	Measured SNR-NEΔT at nominal
1	0.623	0.088	2.14	47.0	400
2	1.610	0.055	0.129	7.23	125
3	3.784	0.340	300 K	320 K	0.02
4	10.826	1.045	300 K	320 K	0.04
5	12.028	1.055	300 K	320 K	0.05

term'' components. The former is caused by the temperature change inside the PR and roughly has a period of one revolution (approximately 91 min). Thus, the correction for this term can be done by monitoring the temperature. The latter may occur due to gradual degradation of system performance (gain, loss, etc.) and/or failure of some active array elements. Since this term may involve changes in antenna characteristics and telemetry sensors, calibration using an external reference target is required.

1) INTERNAL CALIBRATION

The internal calibration algorithm has been developed using a detailed PR system model that describes the temperature dependence of all system parameters related to the conversion process from count value to the radar received power and finally to the radar reflectivity factor. Preliminary error analysis indicates that the error (3σ) less than 1 dB can be achieved in the estimation of radar reflectivity factor.

2) EXTERNAL CALIBRATION

External calibration of the PR will be performed using an ARC placed at a ground calibration site in Japan (Satake et al. 1995; Kumagai et al. 1995). The ARC will have three functions: radar transponder, radar receiver, and beacon transmitter. To reduce the error caused by the uncertainty of PR antenna beam pointing, a special oversample antenna scan will be used. ARC echo levels obtained from the multiple beam directions allow a precise estimation of the PR antenna pointing and the ''peak'' ARC echo level corresponding to the PR antenna beam center position. The external calibration will be performed every month to estimate the long-term drift of the PR system gain. The result will be accumulated to monitor the long-term trend of PR system parameters. Updated PR calibration factors will be determined based upon a statistical analysis of the trend data.

4. Visible and infrared scanner (VIRS)

The VIRS is a five-channel imaging spectroradiometer with bands in the wavelength range from 0.6 to 12 μm. The VIRS data will be used to study precipitation using visible and IR techniques. It will, in addition, provide a link between the derived precipitation and similar data both historical and contemporaneous from geosynchronous and low earth orbiting sensors.

The VIRS is, in many ways, similar to the Advanced Very High Resolution Radiometer (AVHRR) that has flown since 1978 on the National Oceanic and Atmospheric Administration (NOAA) series of spacecraft in that both have the same center wavelengths and bandwidths. The major differences between the two systems are the 2.11-km nadir IFOV of VIRS in contrast to 1.1 km for the AVHRR and the fact that the VIRS has an onboard solar diffuser for postlaunch calibration of the two reflected solar bands. Performance characteristics of the five VIRS channels, measured during thermal-vacuum testing of the system, are listed in Table 5. The noise equivalent differences in temperature (NEΔTs) listed are for a focal plane temperature of 107 K. Predictions for end-of-life hot (worst case) performance for channel 5 indicate a focal plane temperature of 122 K and an NEΔT of 0.13 K.

a. Scan geometry

An exploded view of the VIRS scanner is shown in Fig. 4. The optics consist of a double-sided paddle wheel scan mirror; a 8.9-cm-diameter Cassegrain telescope; two radiative cooler windows; and a cold focal plane with a spectral filter, aplanat lens, and detector element for each of the five channels. The swath width resulting from the 350-km orbit and a $\pm 45°$ scan is 720 km. Each pixel has a 292-μs integration time, resulting in a triangular response function with an along-scan width of 4.22 km and a half-width (IFOV) of 2.11 km at nadir. At the 45° scan angle, the IFOV grows to 3.02 km in both the cross- and along-track directions. The scan lines are contiguous at nadir and, therefore, overlap by approximately 0.9 km at the edge of the swath. The focal plane views 54.18 mrad in the cross-track direction at any instant. This represents the five IFOVs of 6.02 mrad each and a space between each of 6.02 mrad. Therefore, the pixel observed by the first detector on the focal plane is viewed by the fifth detector 2.33 ms later. These delays are removed and the channels are coregistered to approximately 0.2 pixel during ground processing.

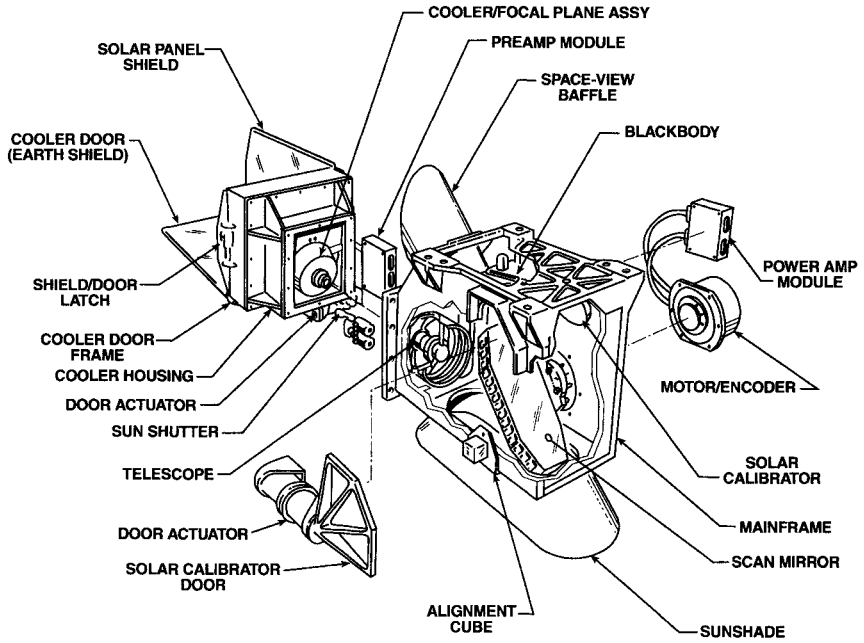

FIG. 4. Detailed view of Visible Infrared Scanner.

b. Onboard calibration

Radiometric calibration of VIRS can be divided into reflected solar and thermal techniques. The reflected solar channels (1 and 2) will initially use counts to radiance conversion developed by viewing a well-calibrated integrating sphere during ground testing. New parameters will be determined periodically using views of the sun via an onboard solar diffuser. The data from the diffuser are collected for each scan line, but the diffuser remains covered by a commandable door (see Fig. 4) except during calibration events. Any degradation in the bidirectional reflectance distribution function (BRDF) of the diffuser will be determined by observing the moon directly through the space view port a few times a year. For VIRS, the moon will act as a source of known reflectance (Keiffer and Wildey 1996) with corrections for lunar phase angle, lunar libration, and earth/sun and earth/moon distance. Response differences observed while viewing the sun via the diffuser and the sun via the moon can be attributed to degradation of the diffuser. With a diameter that is twice the field of view of VIRS, the moon will also provide a means of determining the VIRS point spread function on orbit.

Thermal channel (3, 4, and 5) calibration uses an onboard blackbody that has been characterized via a laboratory blackbody before launch and a view of space to provide a gain and offset for each scan line. Any nonlinearity in the system is determined prelaunch and assumed constant for the life of the mission. This approach is quite similar to that used by AVHRR and other thermal radiometers.

c. Level 1B algorithms

The level 1B output for VIRS will consist of spatially registered, geometrically located pixels with values of band-centered spectral radiance for each channel. For channels 1 and 2, the solar radiance coming from the diffuser will be calculated and, together with the difference in digital counts observed at the diffuser and the space view, will be used to determine a system gain (counts/radiance) for each channel. This gain will be divided into the earth and space view count difference for each earth view pixel, thereby converting the counts to radiance.

For channels 3, 4, and 5, the spectral radiance from the onboard blackbody will be computed using its physical temperature and emissivity. Small corrections will be made for radiance from the scan cavity reflected off the blackbody and into the VIRS. This radiance, as with channels 1 and 2, will be used with the difference in counts between the blackbody and space view to generate gains that will be applied to the earth view counts to convert to radiance. Unlike the reflected solar band gains that will be updated weekly to monthly, the thermal band gains will be recalculated each scan line.

There is a small (2%–5%) change in spectral reflectivity and emissivity with angle of incidence on the scan mirror. A correction will be applied to each of the 261 pixels across the earth view swath for each of the five channels. Finally, since there is a slight dependence of gain on electronics temperature (Barnes et al. 1996), the algorithms for both the reflected solar and thermal channels have a small temperature correction term.

5. Summary

The three primary rainfall instruments aboard TRMM will operate almost continuously during the entire 3-yr mission. Notable exceptions are the occasional external PR calibrations discussed in section 3e and spacecraft yaw maneuvers needed to keep the satellite coolers away from direct sunlight. While the instruments will continue to operate during the yaw maneuvers, these data should not be considered in generating standard geophysical products, as incidence angles and scan geometries will be vastly different from those described here.

The standard data product (level 1B products as defined by EOSDIS) will be generated by the TRMM Data and Information System and then delivered to EOSDIS for dissemination to the scientific community. It is expected that all the data will be routinely available approximately 6 months after the launch of the satellite. This period will be used by the TRMM science team and the TRMM instrument scientists to analyze the data to ensure that sensors are properly calibrated and that the processing software is working as anticipated.

REFERENCES

Barnes, W. L., R. A. Barnes, and A. W. Holmes, 1996: Characterization and calibration results from the Visible and Infrared Scanner (VIRS) for the Tropical Rainfall Measuring Mission (TRMM). *SPIE,* **2957,** 266–276.

Goodman, S. J., and Coauthors, 1996: The optical transient detector: First results. Preprints, *Eighth Conf. on Satellite Meteorology*, Atlanta, GA, Amer. Meteor. Soc., 583–587.

Keiffer, H. H., and R. L. Wildey, 1996: Establishing the moon as a spectral radiance standard. *J. Atmos. Oceanic Technol.,* **13,** 360–375.

Kumagai, H., T. Kozu, M. Satake, H. Hanado, and K. Okamoto, 1995: Development of an active radar calibrator for the TRMM precipitation radar. *IEEE Trans. Geosci. Remote Sens.,* **GE-33,** 1316–1318.

Meneghini, R., and T. Kozu, 1990: *Spaceborne Weather Radar*. Artech House, 199 pp.

Okamoto, K., and T. Kozu, 1993: TRMM precipitation radar algorithms. *Proc. IGARSS'93,* Tokyo, Japan, IEEE Geoscience and Remote Sensing Society, 426–428.

Satake, M., K. Oshimura, Y. Ishido, S. Kawase, and T. Kozu, 1995: TRMM PR data processing and calibration to be performed by NASDA. *Proc. IGARSS'95*, Florence, Italy, IEEE Geoscience and Remote Sensing Society, 57–59.

Simpson, J., C. Kummerow, W.-K. Tao, and R. F. Adler, 1996: On the Tropical Rainfall Measuring Mission (TRMM). *Meteor. Atmos. Phys.,* **60,** 19–36.

Wielicki, B. A., B. R. Barkstrom, E. F. Harrison, R. B. Lee, G. L. Smith, and J. E. Cooper, 1996: Clouds and the Earth's Radiant Energy System (CERES): An earth observing system experiment. *Bull. Amer. Meteor. Soc.,* **77,** 853–868.